

# Anomaly separation of La, Ce and Nd in Se-Chahun iron ore deposit, Bafq district, central Iran

Mohammadali Sarparandeh  
Department of mining and  
metallurgical engineering  
Amirkabir university of  
technology  
Tehran, Iran

Ardeshir Hezarkhani  
Department of mining and  
metallurgical engineering  
Amirkabir University of  
technology  
Tehran, Iran

Bashir Shokouh Saljooghi  
Department of mining and  
metallurgical engineering  
Amirkabir University of  
technology  
Tehran, Iran

**Abstract:** Increase in global prices of rare earth elements (REEs) in recent years has attracted many exploration researchers, especially in Iran. There are some promising areas in central Iran which contain significant amounts of light rare earth elements (LREE). Se-Chahun metasomatic iron ore deposit is one of them. Concentrations of La, Ce and Nd are considerable in some parts of this deposit. On the other hand, one of the most important steps in geochemical exploration of precious elements is separation of anomaly from background. For this purpose, some methods such as classical statistics and fractal models are common. However, application and simplicity are the two main parameters for choosing a proper method. In this study, classical statistics approach (using the mean and standard deviation), and also probability graph and C-A fractal model (Concentration Area) were applied for anomaly-background separation of La, Ce and Nd. Comparing the results of the methods with mineralogy and chemistry of the samples, showed that probability graph had the best performance in anomaly separation. Therefore, considering the results as well as simplicity of the method, it concluded that probability graph is more applicable and a better approach in comparison to others.

**Keywords:** classical statistics; probability graph; C-A fractal; anomaly separation of REEs; Se-Chahun; Central Iran

## 1. INTRODUCTION

Kiruna-type iron ore deposit of Se-Chahun is enriched in light rare earth elements (LREEs) including La, Ce and Nd. Some studies on Kiruna-type iron oxide-apatite (IOA) deposits in Bafq mining district showed the potential for REEs (i.e. Se-Chahun [5, 35]; Choghart: [34, 37]. In addition, some numerical models were applied to predict the hidden patterns of REEs in Choghart iron ore deposit [34, 46]. The REEs are mainly concentrated in specific types of rocks and deposits. Moreover, they are potentially known as an important by-product of iron oxide-apatite (IOA) deposits [39]. Apatite is the main mineral of REEs in the study area. Furthermore, there are some amounts of monazite. Fleischer and Altschuler [16] showed that in apatites from granitic rocks and granitic pegmatites, Ce is dominant, but some analysis showed maximum amounts of Nd, Gd, Dy, or Yb. In anomaly X of Se-Chahun, Ce, Nd and La are more abundant among all REEs. It should be noted that principally, all deposits contain much more LREE than HREE. Most of the deposits have only few percentages of yttrium and other HREEs [36].

Separation of geochemical anomalies from background is one of the important steps in geochemical explorations. Statistical analysis methods play an important role in separating anomalies from background. These methods focus on the frequency distribution of concentrations [20]. Traditional way of anomaly separation is to use the sum of mean ( $\mu$ ) and standard deviation (S) as the threshold. This method is still used as a practical way. In geochemical explorations, values within the ranges  $\mu \pm S$  or  $\mu \pm 2S$  are usually defined as the background [1, 3, 6, 19, 32, 38].

Probability graph is one of the best graphical displays of geochemical distributions, which has been originally introduced to geochemists by Tennant and White [42] (quoted from [32]). This method has been used widely by researchers (for example: [1, 33, 40, 45 and others]).

Since Mandelbrot's invention of the concept of fractals [23], fractal and multi-fractal models have been applied for

separation of anomaly from background values. Main applicable fractal models are Concentration–Area model (C–A: [7]), Spectrum–Area model (S–A: [10]), Multi-fractal Singular Value Decomposition (MSVD: [21]), Concentration–Distance (C–D) model [20], mapping singularity technique [11, 12]. These methods are gradually being adopted as an effective and efficient means to analyze the spatial structures in metallic geochemical systems. In this regard, Mahvash Mohammadi, et al. [22] applied the concentration–area model (C–A) to separate the anomaly from background in Khooni mineral district (Central Iran). They compared the results of C–A fractal with U-statistic method and showed that the U-statistics method has performed better than C–A method.

Though it has been some decades since the development of fractal methods, and even before that the classical statistics, geostatistics and probability graph methods were common, yet the use and preference of these methods are debatable. In the past few decades, many articles were dedicated to usage and preference of fractal methods. Considerable group of researchers believe that these methods are more accurate and precise because of considering data geometry. They have presented many different case studies as examples and proofs for this idea. In comparison, lots of researchers insist on the simplicity and usability of classic methods. In the cases with low data volume and low complexity of dataset, they make an obvious assumption that the simplest method gives more accurate and more real responses. But the first group, based on the literature review and conducted studies, believe in the absolute preference of fractal methods.

The current study, without any orientation, argues about the use of both approaches: 1- traditional methods ( $\mu+nS$  and probability graph) and 2- C-A fractal method. The studied elements are rare earths including La, Ce and Nd, which are usually correlated with each other because of their chemical similarity. They usually form with each other. It is notable that studied deposit has been enriched due to the secondary processes and the effect of metasomatic fluids. The abundant of actinolite is a confirmation for metasomatism.

In this study, 42 bulk lithology samples were collected from anomaly X of Se-Chahun iron ore deposit. They are from pit 1, 2 and 4 (supplementary part of pit 2 is known as pit 4, Figure 1). Samples were taken from ore body and metasomatic host rock. After preparing and analysis of the samples, three methods (i.e. classical statistics based on the mean and standard deviation, probability graph and C-A fractal model) were applied for anomaly-background separation of La, Ce and Nd.

## 2. GEOLOGICAL SETTINGS OF STUDY AREA

The Bafq district, extending from Bafq to Saghand, is part of the central Iranian micro plate which is now embedded within the Alpine-Himalayan orogenic system. This district is located in central Iran and is between 31°, 30' to 32°, 45' north latitude and 55°, 20' to 55°, 50' east longitude [44]. The central Iranian terrane is divided into three major crustal domains, from east to west: the Lut Block, Tabas Block and the Yazd Block [2]. The Tabas and Yazd blocks are separated by a nearly 600 km long, 80 km wide, arcuate and structurally complex belt (Kashmar-Kerman Tectonic Zone) composed of variably deformed and fault-bound supracrustal rocks [31]. Bafq mining district hosts several Kiruna-type iron oxide-apatite (IOA) deposits such as Se-Chahun, Choghart, Chahgaz, Esfordi, Mishdovan [4, 14, 46]. The Early Cambrian igneous rocks of the Bafq mining district have a bimodal nature. The chondrite-normalized REEs patterns display significant variation from LREEs to HREEs with no considerable Eu anomalies for basaltic rocks, and show obvious enrichment in the LREEs with important negative Eu anomalies for the rhyolitic domes [30]. The REEs enrichment is intensely associated with the formation of phosphate minerals in many IOA deposits. However, sometimes bastnasite and allanite are significant [28]. Edfelt [15] explained that there are few complications in the phosphate-REE relationship in some Kiruna districts. Hence, the relationship between REEs and phosphate minerals in such deposits should be more understood. In these deposits, apatites characteristically comprise 2000–6000 ppm REEs [17, 18]. Daliran [13] claimed that Bafq district apatites contain up to 1.75 wt. % REEs. Some researches present that post-depositional REE leaching could be occurred in apatite in which the inclusions of monazite and xenotime might be seen [5, 41, 43]. The U–Pb dating of monazite inclusions in apatite demonstrates that the REEs redistribution in apatite might be happened frequently throughout hydrothermal processes several million years after the formation of the IOA deposits [41].

The Se–Chahun deposit is composed of two major groups of ore bodies called the X and XI anomalies [26]. Anomaly X contains 11 Mt iron ore reserve with mainly rich magnetite ore [44]. Anomaly XI occurs 3 km northeast of anomaly X. Each anomaly consists of two or three smaller tabular to lens shaped ore bodies in association with other small bodies [5]. The mineralization is mainly hosted by metasomatized tuffs of andesite composition. Host rocks are known as metasomatites in this deposit [26]. The ore bodies map (anomaly X of Se-Chahun deposit), as well as the location of samples within the study area are shown in Figure 1.

The host rocks have a gradual boundary. Samples mainly include iron ores, low-grade ores (transition zone, consisting of plagioclase and actinolite) and metasomatitic rocks (mainly consists of actinolite and plagioclase). The host rocks are composed of metasomatized andesitic tuffs. Limestones and dolomites are observed in limited areas. Ore body is

comprised of high grade magnetite. The most important REE-bearing minerals in Se-Chahun deposit are apatite and monazite. The content of rare earth elements is directly related to the amount of apatite. The more the apatite, the more REE is. Monazites are very fine grained and just can be distinguished in SEM images.

## 3. GEOCHEMICAL DATASET

42 samples were taken from Se-Chahun iron ore deposit. The strategy of sampling was bulk lithology sampling with least number of samples (to consider the cost) which shows the most variances and the most features and reality of the deposit. They are about 1 to 1.5 kg weight and have been taken from ore body and metasomatic host rock. After preparation, samples were analyzed with Inductively Coupled Plasma Mass Spectrometry (ICP-MS). Concentrations of La, Ce, Nd, P and some statistical parameters of these elements and logarithmic value of them are shown in Table 1. La, Ce and Nd are the most concentrated elements among all REEs. Histograms of them are illustrated in Figure 2. Normal Q-Q plots of Ln (La), Ln (Ce) and Ln (Nd) show lognormal distribution of them (Figure 3). In addition, after taking logarithms, because of logarithmic distribution of data, histograms with normal curves were drawn once more (Figure 4).

## 4. METHODOLOGY

The first method which was applied in this study is the traditional method for separation of anomaly from background (i.e. using mean ( $\mu$ ) and standard deviation ( $S$ )). In this regard, values upper than  $\mu+S$  and  $\mu+2S$  were defined as anomaly and High anomaly, respectively. Another approach for dividing the populations (or anomaly background separation) is probability graph. In this method, cumulative frequency curve is plotted on a logarithmic graph and a change in the slope of the curve or point of inflection indicates the presence of more than one distribution [45]. For this purpose, cumulative frequencies of each element (in percent) were calculated in logarithmic distances and then, they were plotted on the logarithmic graphs. On the other hand, C-A fractal model was applied as the third approach. The C-A fractal [7, 8, 9] is one of the most widely used fractal models. The C-A model, originally developed by Cheng et al. [7], represents the first important step in fractal/multifractal modeling of geochemical data and has been “a fundamental technique for modeling of geochemical anomalies” [6, 25, 29]. The expression is given in Eq. (1).

$$A(\geq c) \propto c^{-\alpha} \quad (1)$$

In this model, the measure  $A(\geq c)$  is the area enclosed by contours with values greater than or equal to  $c$  on a geochemical contour map. It can also be estimated using box-counting techniques, which involves counting the number of pixels with averaged concentration values greater than or equal to  $c$  on interpolated geochemical images. The exponent  $\alpha$  may have different values for different ranges of  $c$ . If the geochemical data is composed of multiple populations (for example, a mineralization-related anomalous population and a background population), the distribution of the points on a log  $A(\geq c)$ -log ( $c$ ) plot fits more than one line segment. Each line segment is presumed to represent a different population characterized by a different value of the exponent  $\alpha$ . The right-most breakpoint joining the line segments is generally taken as the threshold for separating anomaly from background [9, 24, 27, 29].

## 5. RESULTS AND DISCUSSION

Because of lognormal nature of dataset, which has been discussed in section 3, logarithmic values of the concentrations of La, Ce and Nd were used in method of classical statistics. Consequently, using  $\mu+S$  and  $\mu+2S$  as the thresholds, anomaly and high anomaly zones, were determined (Table 2). The average values of La, Ce and Nd as well as the number of samples for each zone are illustrated in Table 2. As it can be seen in Table 2, the threshold of  $\mu+2S$  has separated just 2 samples for La and 1 sample for Ce and Nd, with highest concentrations. Therefore, it seems to be more reasonable to use  $\mu+S$  as the threshold.

Cumulative probability graphs for La, Ce and Nd were plotted and showed in Figure 5. Intervals are logarithmic and the lower limit of each class was plotted. It is possible to identify the populations of the same samples by such graphs. However, in this study, the purpose is to determine the appropriate thresholds for anomaly-background separation. The thresholds for anomalies were found visually on these graphs. These points were determined with changes in the slopes of the curves at the ends. The thresholds are 90.1, 148.5 and 90.1 ppm for La, Ce and Nd, respectively. The averages of La, Ce and Nd in anomalous parts are 257.7, 500.5 and 247.5 ppm, respectively. By applying these thresholds, anomalies were determined. A summary of this method is illustrated in Table 3.

Distribution maps of La, Ce and Nd are shown in Figure 6. These maps were plotted based on the samples and interpolation using inverse distance method. Red color demonstrates the anomalous areas and highest concentrations and in contrast blue color represents the background areas with least concentrations. As it can be seen, the most concentrated area is located in south part in pit 4. Figure 7 shows the log-log plots of Concentration-Area for La, Ce and Nd with determined thresholds of anomaly zones. Moreover, Anomalies which have been resulted by fractal model and threshold value corresponding to each one, are illustrated in Table 4. The thresholds were determined in points where the

## 6. CONCLUSION

Whatever the variance is lower, the outputs of methods will be closer together. Nd has more similar results in the three methods because of its lower variance. The amount of variance in the study area is high. Therefore, for anomaly-background separation of REEs in this area, it is important to find an appropriate method. Results of probability graph have the best matches with geological and experimental information in comparison to traditional method of using  $\mu+S$

slopes are changed from the ends of the curves. They are 106.4, 244.7 and 111.2 ppm for La, Ce and Nd, respectively. In addition, the averages of La, Ce and Nd in anomalous parts are 452.2, 798 and 295.2 ppm, respectively.

A comparison between all three methods can be seen with a quick look in Table 5. Finally, the validity of each of these methods is possible only by comparing the geological information. For that matter, the results were compared with geological surveys and field studies as well as experimental analysis of samples such as XDR and microscopic analysis. As a conclusion and summary of findings, 10 samples that were determined as the anomaly by all three methods, were collected in Table 6. It should be noted that all of these samples have anomalous condition and almost they are all of the anomalous samples. Geological studies show that REEs of Se-Chahun deposit are mainly in apatite and some amounts in monazite. These minerals were detected in 9 of these 10 samples (Table 6). Some apatites are depleted from REEs, as it has been discussed by Bonyadi et al. [5]. However, all of the 10 samples, more or less, have considerable amounts of La, Ce and Nd. Therefore, it can be concluded that all three methods, have shown the anomaly correctly. But, probability graph identified completely and fractal model identified samples with higher concentrations in comparison to others. In addition, anomaly and the changes in the slopes of the curves are more recognizable in probability graphs comparing with Concentration-Area plots. Results of Nd have the most similarity in the three methods. This element has the least variance.

The results showed that at least in cases such as this study, in which there are few number of data, more simple methods have the more appropriate responses. Though some researchers consider this a fact, lots of others use the articles of fractal methods as a basis to their studies, and insist on it. But this study showed that this hypothesis is not always correct. The probability graph provided more accurate answers, which are consistent with the geological evidences that are summarized in Table 6.

and  $\mu+2S$  as well as C-A fractal model. According to results and simplicity of the method, probability graph is more applicable and better approach in comparison to others. Moreover, it concluded that in cases, which there are few number of data, more simple methods have the more appropriate responses.

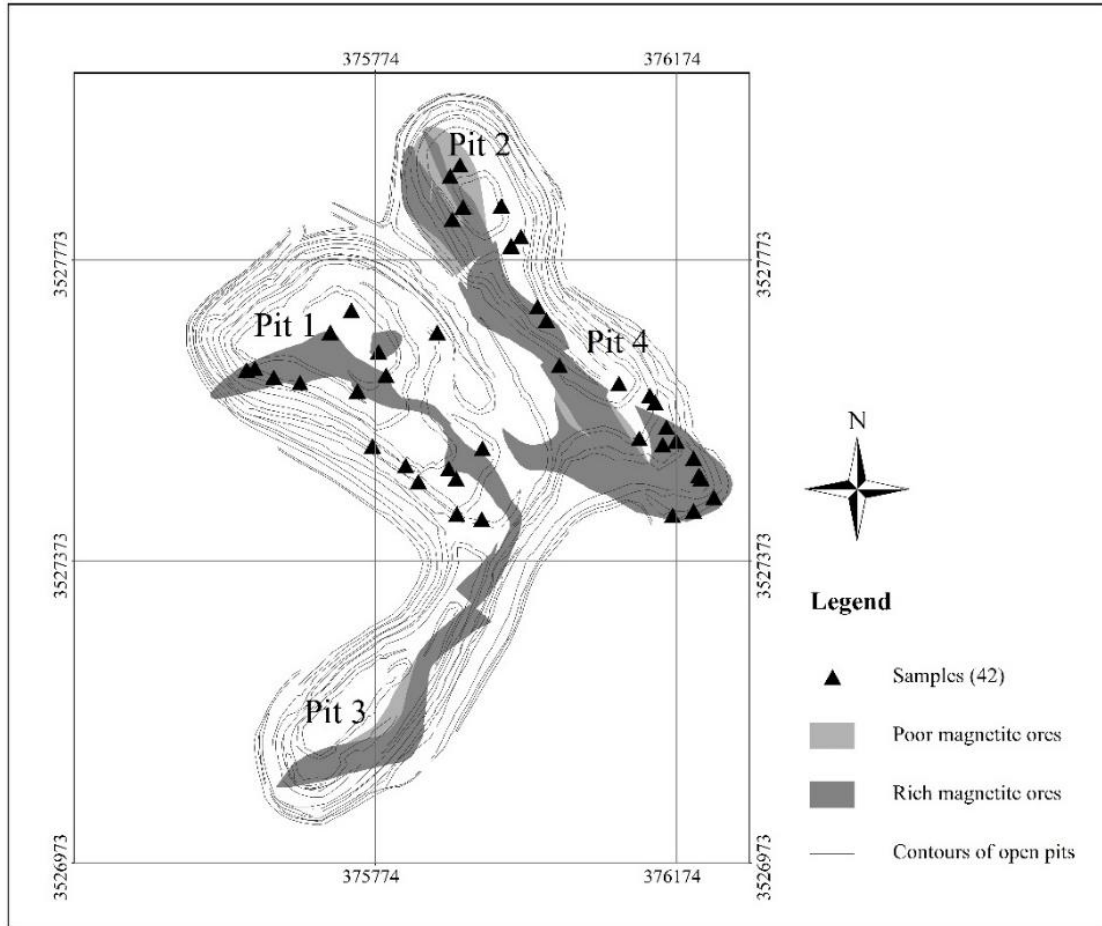


Figure 1 Ore bodies (anomaly X of Se-Chahun deposit), and sample locations. Contours of open pits are shown in the map and the open pits are numbered from 1 to 4 (supplementary part of pit 2 is known as pit 4) (modified after [26]).

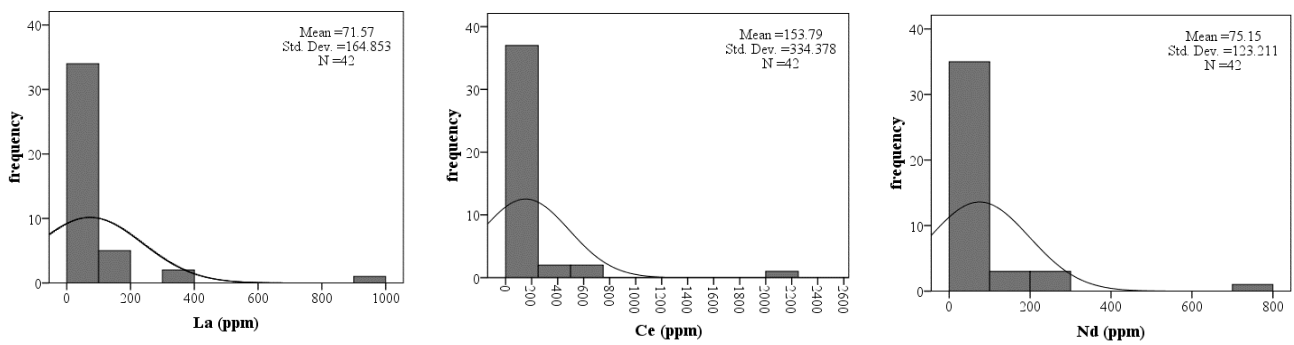


Figure 2 Histograms of La, Ce and Nd with distribution curves (42 samples).

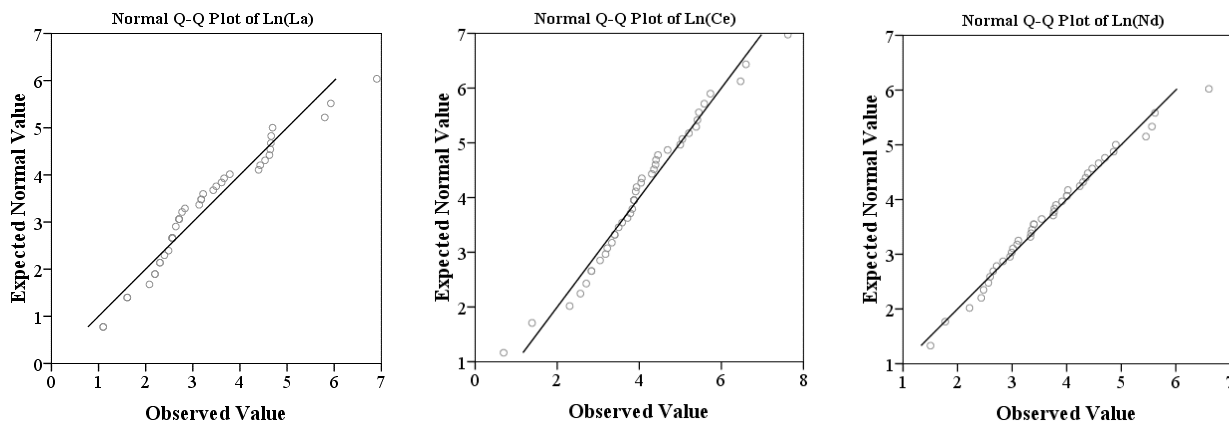


Figure 3 Normal Q-Q plots for logarithmic values of La, Ce and Nd. Plots show the lognormal distribution.

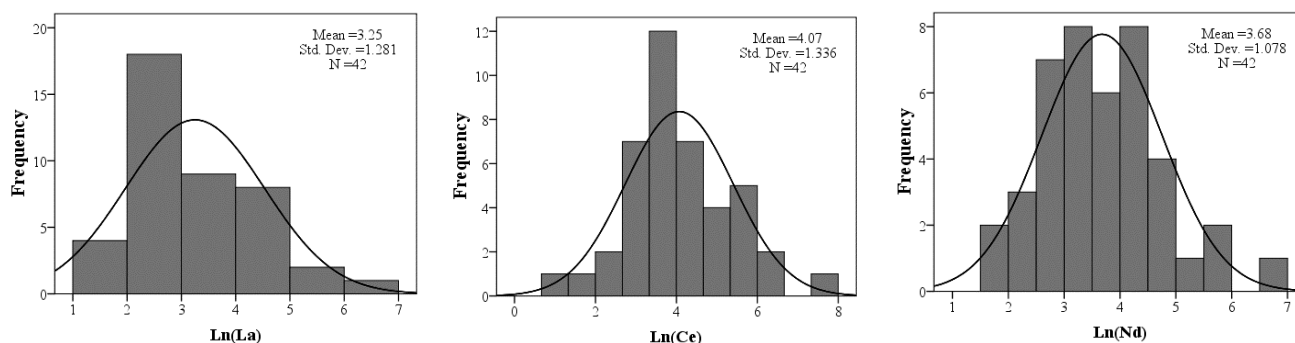


Figure 4 Histograms of La, Ce and Nd (logarithmic data) with distribution curves.

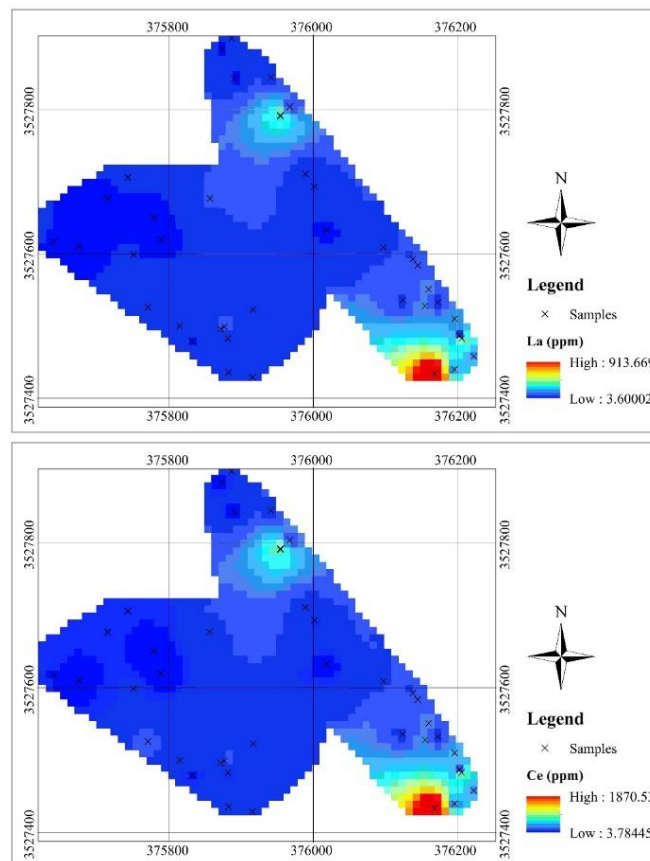
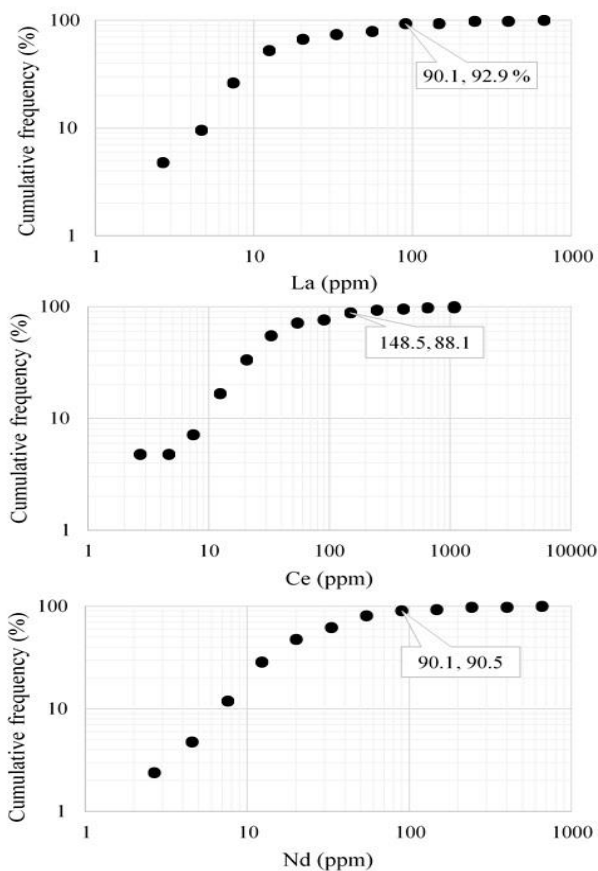


Figure 5 Cumulative probability graphs of La, Ce and Nd with thresholds of anomaly zones.

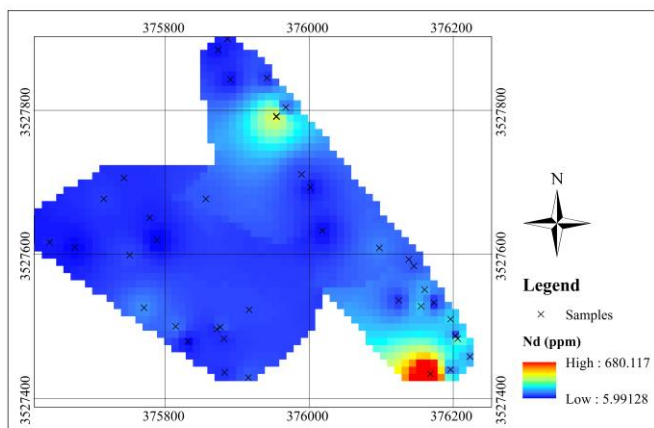


Figure 6 Distribution maps of La, Ce and Nd, based on the samples (Interpolation by inverse distance method).

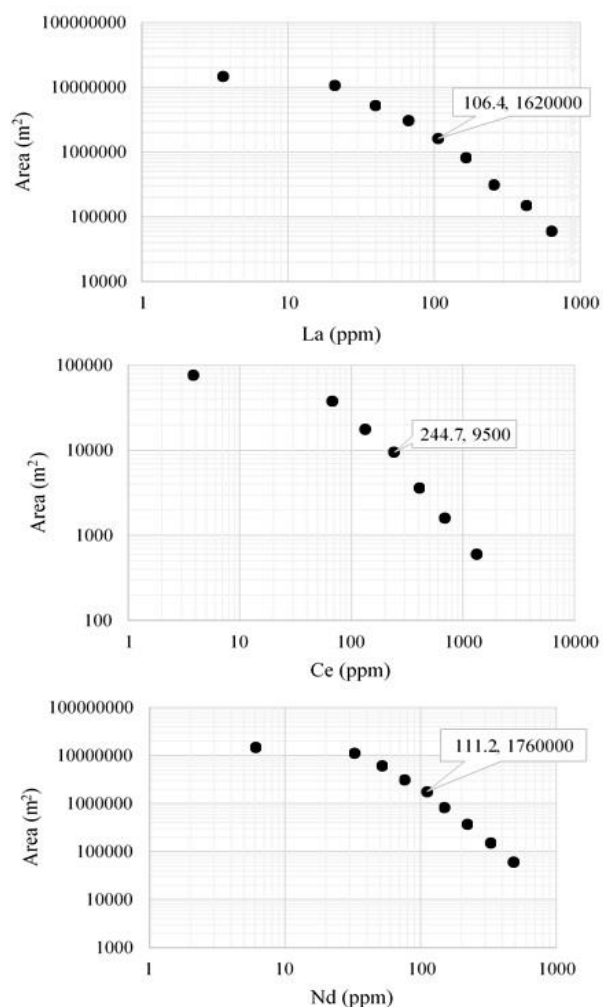


Figure 7 Concentration-Area plots of La, Ce and Nd with determined thresholds of anomaly zones.

Table 1 Assayed REEs and some statistical parameters.

| Elements (ppm)     | La  | Ce   | Nd  | Ln(La) | Ln(Ce) | Ln(Nd) |
|--------------------|-----|------|-----|--------|--------|--------|
| Mean               | 72  | 154  | 75  | 3.25   | 4.07   | 3.68   |
| Median             | 17  | 49   | 39  | 2.8    | 3.89   | 3.65   |
| Variance           | 271 | 1118 | 151 | 1.64   | 1.78   | 1.16   |
| Standard deviation | 165 | 334  | 123 | 1.28   | 1.34   | 1.08   |
| Minimum            | 3   | 2    | 5   | 1.1    | 0.69   | 1.5    |
| Maximum            | 995 | 2037 | 740 | 6.9    | 7.62   | 6.61   |
| Skewness           | 5   | 5    | 4   | 0.8    | 0.18   | 0.43   |
| Kurtosis           | 25  | 26   | 21  | 0.575  | 0.91   | 0.28   |

Table 2 Results of classical statistics using  $\mu+S$  and  $\mu+2S$  as the thresholds for anomaly and high anomaly.

|          | Ln(La) | Ln(Ce) | Ln(Nd) |
|----------|--------|--------|--------|
| $\mu+S$  | 4.53   | 5.41   | 4.75   |
| $\mu+2S$ | 5.81   | 6.74   | 5.83   |

| Element | Range        | Threshold | Mean (ppm) | Number of samples |
|---------|--------------|-----------|------------|-------------------|
| La      | Anomaly      | 92.9      | 257.7      | 9                 |
|         | High anomaly | 334.6     | 685        | 2                 |
| Ce      | Anomaly      | 222.9     | 635.4      | 7                 |
|         | High anomaly | 847.9     | 2037       | 1                 |
| Nd      | Anomaly      | 116       | 295.2      | 6                 |
|         | High anomaly | 341       | 739.5      | 1                 |

Table 3 The resulted anomalies by probability graphs.

| Element | Threshold | Mean (ppm) | Number of samples |
|---------|-----------|------------|-------------------|
| La      | 90.1      | 257.7      | 9                 |
| Ce      | 145.5     | 500.5      | 10                |
| Nd      | 90.1      | 247.5      | 8                 |

Table 4 Anomalies which have been resulted by fractal model

| Element | Threshold | Mean (ppm) | Number of samples |
|---------|-----------|------------|-------------------|
| La      | 106.4     | 452.2      | 4                 |
| Ce      | 244.7     | 798        | 5                 |
| Nd      | 111.2     | 295.2      | 6                 |

Table 5 Comparison between three methods.

| Element | M+S       |            |     | Probability graph |            |     | Fractal model |            |     |
|---------|-----------|------------|-----|-------------------|------------|-----|---------------|------------|-----|
|         | Threshold | Mean (ppm) | No. | Threshold         | Mean (ppm) | No. | Threshold     | Mean (ppm) | No. |
| La      | 92.9      | 257.7      | 9   | 90.1              | 257.7      | 9   | 106.4         | 452.2      | 4   |
| Ce      | 222.9     | 635.4      | 7   | 145.5             | 500.5      | 10  | 244.7         | 798        | 5   |
| Nd      | 116       | 295.2      | 6   | 90.1              | 247.5      | 8   | 111.2         | 295.2      | 6   |

Table 6 Concentration of La, Ce and Nd in all determined anomaly samples with detection of apatite and monazite by XRD and SEM methods (\* marked concentrations are under the thresholds).

| Sample code | La (ppm) | Ce (ppm) | Nd (ppm) | Apatite (XRD) | Apatite (SEM) | Monazite (SEM) |
|-------------|----------|----------|----------|---------------|---------------|----------------|
| 1-19        | 84*      | 156      | 77.3*    | –             | Not checked   | Not checked    |
| 2-6         | 109      | 309      | 260.3    | –             | –             | ✓              |
| 2-9         | 375      | 734      | 275.3    | ✓             | Not checked   | Not checked    |
| 4-1         | 330      | 644      | 233      | ✓             | –             | ✓              |
| 4-3         | 104      | 266      | 134.3    | ✓             | ✓             | ✓              |
| 4-5         | 995      | 2037     | 739.5    | ✓             | ✓             | ✓              |
| 4-6         | 93       | 183      | 69.4*    | ✓             | ✓             | ✓              |
| 4-7         | 106      | 225      | 98.1     | ✓             | –             | –              |
| 4-9         | 102      | 218      | 110.2    | ✓             | ✓             | ✓              |
| 4-10        | 105      | 233      | 128.9    | ✓             | ✓             | ✓              |

## 7. REFERENCES

- [1] Abd El Nabi, S.H. (2001). Evaluation of airborne gamma-ray spectrometric data for the Missikat uranium deposit, Eastern Desert, Egypt. *Applied Radiation and Isotopes*, 54, 497–507.
- [2] Alavi, M. (1991). Tectonic map of the Middle East (scale 1:5, 000, 000). Geological Survey of Iran.
- [3] Ander, E.L., Johnson, C.C., Cave, M.R. et al. (2013). Methodology for the determination of normal background concentrations of contaminants in English soil. *Science of the Total Environment*, 454–455, 604–618.
- [4] Barton, M.D. (2014). Iron oxide(-Cu-Au-REE-P-Ag-U-Co) systems. *Treatise on Geochemistry*, 13, 515-541.
- [5] Bonyadi, Z., Davidson, G.J. Mehrabi, B. et al. (2011). Significance of apatite REE depletion and monazite inclusions in the brecciated Se-Chahun iron oxide apatite deposit, Bafq district, Iran: insights from para-genesis and geochemistry. *Chemical Geology*, 281, 253–269.
- [6] Carranza, E.J.M. (2009). Geochemical anomaly and mineral prospectivity mapping in GIS. *Handbook of exploration and environmental geochemistry* (M. Hale, Editor), 11, 51–84.
- [7] Cheng, Q., Agterberg, F.P., Ballantyne, S.B. (1994). The separation of geochemical anomalies from background by fractal methods. *Journal of Geochemical Exploration*, 51, 109–130.
- [8] Cheng, Q., Agterberg, F., Bonham-Carter, G. (1996). A spatial analysis method for geochemical anomaly separation. *Journal of Geochemical Exploration*, 56, 183–195.
- [9] Cheng, Q., (1999). Spatial and scaling modelling for geochemical anomaly separation. *Journal of Geochemical Exploration*, 65, 175–194.
- [10] Cheng, Q., Xu, Y., Grunsky, E. (2000). Integrated spatial and spectrum method for geochemical anomaly separation. *Natural Resources Research*, 9, 43–51.
- [11] Cheng, Q. (2007). Mapping singularities with stream sediment geochemical data for prediction of undiscovered mineral deposits in Gejiu, Yunnan Province, China. *Ore Geology Reviews*, 32, 314–324.
- [12] Cheng, Q. (2008). Non-linear theory and power-law models for information integration and mineral resources quantitative assessments. *Mathematical Geosciences*, 40, 503–532.
- [13] Daliran, F. (2002). Kiruna-type iron oxide-apatite ores and apatites of the Bafq district, Iran, with an emphasis on the REE geochemistry of their apatites. *Hydrothermal iron oxide copper-gold & related deposits: a global perspective*, 2, 303–320.
- [14] Daliran F., Stosch H.G., Williams P.J., et al. (2010). Lower cambrian iron oxide-apatite-REE (U) deposits of the Bafq district, east-central Iran. *Exploring for iron oxide copper-gold deposits: Canada and global analogues*, Geological Association of Canada, Short Course Notes 20, 143–155.
- [15] Edfelt, A. (2007). The Tjarrojakka apatite-iron and Cu (-Au) deposits, northern Sweden: products of one ore

- forming event. Dissertation, Lulea University of Technology, Sweden.
- [16] Fleischer, M. (1969). The lanthanide elements in fluorite. *Indian Mineral*, 10, 36-39.
- [17] Frietsch, R. (1982). On the chemical composition of the ore breccia at Luossavaara, northern Sweden. *Mineralium Deposita*, 17, 239-243.
- [18] Frietsch, R., Perdahl, J.A. (1995). Rare earth elements in apatite and magnetite in Kiruna-type iron ores and some other iron ore types. *Ore Geology Reviews*, 9, 489-510.
- [19] Galuszka, A. and Migaszewski, Z.M. (2011). Geochemical background – an environmental perspective. *Mineralogia*, 42 (1), 7-17.
- [20] Li, C., Ma, T. and Shi, J. (2003). Application of a fractal method relating concentration and distances for separation of geochemical anomalies from background. *Journal of Geochemical Exploration*, 77, 167-175.
- [21] Li, Q. and Cheng, Q. (2004). Fractal singular-value (eigenvalue) decomposition method for geophysical and geochemical anomaly reconstruction. *Earth Science-Journal of China University of Geosciences*, 29, 109-118 (in Chinese with English abstract).
- [22] Mahvash Mohammadi, N., Hezarkhani, A., Shokouh Saljooghi, B. (2016). Separation of a geochemical anomaly from background by fractal and U-statistic methods, a case study: Khooni district, Central Iran. *Chemie der Erde*, 76, 491-499.
- [23] Mandelbrot, B.B., Passoja, D.E., Paullay, A.J. (1984). Fractal character of fracture surfaces of metals. *Nature*, 308, 721-722.
- [24] Meigoony, M.S., Afzal, P., Gholinejad, M. et al. (2014). Delineation of geochemical anomalies using factor analysis and multifractal modeling based on stream sediments data in Sarajeh 1: 100,000 sheet, Central Iran. *Arabian Journal of Geosciences*, 7, 5333-5343.
- [25] Mokhtari, Z., Boomeri, M., Bagheri, S. (2015). Application of multifractal modeling technique in systematic litho-geochemical survey to identify Au-Cu anomalies in the Siah-Jangal area, Southeastern of Iran. *Arabian Journal of Geosciences*, 8, 9517-9530.
- [26] National Iranian Steel Corporation (1975). Report on detailed exploration of Se-Chahun iron ore deposit in central Iran. Tehran, National Iranian Steel Corporation (NISCO).
- [27] Nazarpour, A., Omran, N.R., Paydar, G.R. et al. (2015). Application of classical statistics, logratio transformation and multifractal approaches to delineate geochemical anomalies in the Zarshuran gold district, NW Iran. *Chemie der Erde-Geochemistry*, 75, 117-132.
- [28] Oreskes, N., Einaudi, M.T. (1990). Origin of rare earth element-enriched hematite breccias at the Olympic dam Cu-U-Au-Ag deposit, Roxby Downs, South Australia. *Economic Geology*, 85, 1-28.
- [29] Pazand, K., Hezarkhani, A., Ataei, M. et al. (2011). Application of multifractal modeling technique in systematic geochemical stream sediment survey to identify copper anomalies: a case study from Ahar, Azarbaijan, Northwest Iran. *Chemie der Erde-Geochemistry*, 71, 397-402.
- [30] Rajabi, A., Canet, C., Rastad, E., et al. (2015). Basin evolution and stratigraphic correlation of sedimentary-exhalative Zn-Pb deposits of the early cambrian Zarigan-Chahmir basin, Central Iran. *Ore Geology Reviews*, 64, 328-353.
- [31] Ramezani, J., Tucker, R.D. (2003). The saghand region, Central Iran: U-Pb geochronology, petrogenesis and implications for gondwana tectonics. *American Journal of Science*, 303, 622-665.
- [32] Reimann, C., Filzmoser, P., Garrett, R.G. (2005). Background and threshold: critical comparison of methods of determination. *Science of the Total Environment*, 346, 1-16.
- [33] Risdianto, D., Kusnadi, D. (2010). The Application of a Probability Graph in Geothermal Exploration. *Proceedings World Geothermal Congress, Bali, Indonesia, 25-29 April*.
- [34] Sarparandeh, M. and Hezarkhani, A. (2016). Application of self-organizing map for exploration of REEs' deposition. *Open Journal of Geology*, 6, 571-582.
- [35] Sarparandeh, M. and Hezarkhani, A. (2016). Studying distribution of rare earth elements by classifiers, Se-Chahun iron ore, Central Iran. *Acta Geochimica*, 35, 140, 1-8.
- [36] Schuler, D., Buchert, M., Liu, R., et al. (2011). Study on rare earths and their recycling, Final report for the Greens/EFA group in the european parliament, The Greens/European free alliance, 42-59.
- [37] Shekarian, Y. (2014). Geochemical investigations on REEs in N-NE Choghart iron deposit and their economic evaluations. Dissertation, Amirkabir University of Technology (Tehran Polytechnic), Tehran.
- [38] Siegel, F. R. (2002). *Environmental geochemistry of potentially toxic elements*. Springer-Verlag, Berlin, 80-81
- [39] Simandl, G. (2014). Geology and market-dependent significance of rare earth element resources. *Mineralium Deposita*, 49, 889-904.
- [40] Sinclair A.J. (1974). Selection of threshold values in geochemical data using probability graphs. *Journal of Geochemical Exploration*, 3, 129 - 149.
- [41] Stosch, H.G., Romer, R.L., Daliran, F., et al. (2011). Uranium-lead ages of apatite from iron oxide ores of the Bafq district, east-central Iran. *Mineralium Deposita*, 46, 9-21.
- [42] Tennant C.B., White M.L. (1959). Study of the distribution of some geochemical data. *Economic Geology*, 54, 1281- 1290.
- [43] Torab, F., Lehmann, B. (2007). Magnetite-apatite deposits of the Bafq district, central Iran: apatite geochemistry and monazite geochronology. *Mineralogical Magazine*, 71, 347-363.
- [44] Torab, F. (2008). Geochemistry and metallogeny of magnetite apatite deposits of the Bafq mining district, Central Iran. Dissertation, Clausthal University of Technology, Germany.

[45] Williams, X. K. (1967). Statistics in the interpretation of geochemical data. *New Zealand Journal of Geology and Geophysics*, 10 (3), 771–797.

[46] Zaremotlagh, S., Hezarkhani, A. (2016). A geochemical modeling to predict the different concentrations of REE

and their hidden patterns using several supervised learning methods: Choghart iron deposit, bafq, Iran. *Journal of Geochemical Exploration*, 165, 35–48.

f